Howard Hughes Medical Institute

Published as: *Nat Struct Mol Biol*. ; 18(9): 1068–1074.

Mechanism of Actin Filament Nucleation by the Bacterial Effector VopL

Bingke Yu[1,2], **Hui-Chun Cheng**[1,2], **Chad A. Brautigam**[1], **Diana R. Tomchick**[1], and **Michael K. Rosen**[1,2]

[1] Department of Biochemistry, University of Texas Southwestern Medical Center, 5323 Harry Hines Boulevard, Dallas, Texas 75390

[2] Howard Hughes Medical Institute, University of Texas Southwestern Medical Center, 5323 Harry Hines Boulevard, Dallas, Texas 75390

Abstract

Vibrio parahaemolyticus protein L (VopL) is an actin nucleation factor that induces stress fibers when injected by bacteria into eukaryotic host cells. VopL contains three N-terminal Wiskott-Aldrich Homology 2 (WH2) motifs and a unique VopL C-terminal domain (VCD). We describe crystallographic and biochemical analyses of filament nucleation by VopL. The WH2 element of VopL does not nucleate on its own, and requires the VCD for activity. The VCD forms a U-shaped dimer in the crystal, which is stabilized by a terminal coiled-coil. Dimerization of the WH2 motifs contributes strongly to nucleation activity, as do contacts of the VCD to actin. Our data lead to a model where VopL stabilizes primarily lateral (short-pitch) contacts between actin monomers to create the base of a two-stranded filament. Stabilization of lateral contacts may be a common feature of actin filament nucleation by WH2-based factors.

Actin cytoskeletal dynamics are important in numerous cellular processes, including migration, division and maintenance of morphology[1–3]. These functions all require rapid assembly of new actin filaments de novo from actin monomers. However, actin assembly is intrinsically slow, due to kinetic and thermodynamic barriers to forming the actin dimers and trimers needed to initiate filament growth[4]. Cells have therefore developed specialized factors to stabilize these actin nuclei and thus catalyze filament assembly[4]. Three classes of so-called actin nucleation factors have been identified: Arp2/3 complex, formin proteins and WASP Homology domain 2 (WH2)-based nucleators[5–11]. Arp2/3 complex binds to the side of an existing filament and initiates growth of a new filament from its actin related protein 2 (Arp2) and Arp3 subunits[12,13]. Alignment of the actin homologs Arp2 and Arp3 to resemble

Corresponding Author: Dr. Michael K. Rosen, Tel: (214)-645-6361, Fax: (214)-645-6291, Michael.Rosen@UTSouthwestern.edu.

Accession codes

Protein Data Bank code of VCD: 3SEO

Author Contributions

M.K.R. conceived of the project; B.Y. performed the work; C.A.B. and D.R.T. assisted with X-ray diffraction data collection and structure determination. H.-C. C. assisted with designing and making the VopL constructs; M.K.R and B.Y. analyzed the data and wrote the paper.

the first two monomers at the base of an actin filament is believed to be a key aspect of Arp2/3-mediated nucleation[14]. Formin proteins nucleate linear filaments through a conserved formin homology 2 (FH2) domain, which is also thought to organize three actin monomers into a structure that resembles the base of an actin filament[15,16]. After nucleation, formins remain associated with the growing filament barbed end as new monomers are added[5]. Several mechanisms have been proposed to account for this processive activity[15–18]. The WH2-based actin nucleators have been identified most recently, and include Spire, Corbon blue (Cobl) and Leiomodin (Lmod)[7–9,11]. These proteins all contain a series of tandem WH2 motifs, each capable of binding an actin monomer. These proteins are also thought to act through organization of multiple actin monomers into a stable structure that resembles an actin filament. However, the nature of that nucleus—whether the monomers are aligned longitudinally to resemble a single strand of the paired actin filament, or laterally to resemble both strands—appears to differ between the various factors, due to differences in the WH2 domains, the linkers between them and the presence of additional actin-binding elements[7–10,19].

During infection, many bacterial and viral pathogens hijack the actin cytoskeleton of eukaryotic host cells to increase their pathogenicity or mobility[20–22]. In many cases, these pathogens target pathways that control actin filament nucleation[23–28]. Several bacteria have evolved WH2-based actin nucleation factors, which they inject into host cells through type III secretion systems to promote actin assembly. These factors include VopL, VopF, TARP and Sca2[29–33]. VopL and its homolog VopF are effector proteins of the gram negative bacteria *Vibrio parahaemolyticus* and *Vibrio cholera*, respectively[30,32,34]. When introduced into eukaryotic cells, VopL and VopF induce actin stress bers and filopodia, respectively. *In vitro*, both proteins potently induce nucleation of actin filaments that, at least for VopL, grow at their barbed ends[30]. Both consist of one or two proline-rich (P) motifs and three tandem WH2 motifs, followed by either a VopL/VopF C-terminal domain (VCD) that lacks homology to known proteins. Mutagenesis of the WH2 motifs impairs the ability of VopL to induce stress fibers in cells, implicating these elements in actin nucleation[30]. The mechanisms by which the VopL/VopF WH2 motifs and C-terminal domain assemble an actin nucleus remain unclear, as does the relationship between these bacterial proteins and eukaryotic WH2-based nucleation factors.

Here we set out to understand the mechanism of VopL-mediated actin nucleation. To achieve this, we used a combination of biochemical and crystallographic analyses. We show that although the individual WH2 domains can bind actin with nM affinity, the $(WH2)_3$ element (W_3) alone cannot nucleate filaments, and requires the VCD for activity. The VCD is a high affinity dimer in solution and forms a U-shaped dimeric structure in the crystal. Dimerization dramatically enhances filament nucleation by W_3. The VCD alone retains some nucleation activity, which can be decreased by mutation of exposed surfaces, suggesting that the domain contacts actin during nucleation. Our data suggest a model for VopL-mediated nucleation in which contacts of both the WH2 motifs and the VCD stabilize inter-strand contacts between the initial two or more actin monomers to create a filament nucleus.

Results

WH2 motifs and VCD are both needed for actin nucleation

Each WH2 motif in VopL contains both the N-terminal hydrophobic residues and C-terminal basic sequence that are important for binding to actin monomers in eukaryotic WH2 motifs[35]. We used isothermal titration calorimetry to measure the binding affinity of each motif (named WH2a, WH2b and WH2c from N- to C-terminus, Fig. 1a) for monomeric actin (Supplementary Fig. 1). The dissociation equilibrium constants (K_D) range from 5 to 15 nM, explaining the nM potency of VopL in actin assembly assays[30], and indicating little difference between the ability of the motifs to bind actin. Note that these assays were performed in low salt buffer to prevent actin polymerization (see Methods), and affinities could be somewhat different in the presence of higher KCl and $MgCl_2$ concentrations.

Linear WH2 arrays in other nucleation factors such as Spire and Cobl have substantial activity. But a VopL fragment containing only the three WH2 motifs without the VCD (construct W_3) was completely inactive in pyrene-actin assembly assays (Fig. 1b, half times of actin assembly ($t_{1/2}$) are tabulated in Fig. 1a). High concentrations of W_3 inhibited assembly, likely by sequestration of actin monomers (Supplementary Fig. 2). By contrast, the VCD alone retained some actin assembly activity, albeit with ~100-fold lower potency than W_3-C, which contains the three WH2 motifs and the VCD (Figs. 1c, a; 500 nM VCD has activity similar to 5 nM W_3-C (not shown)). To further dissect the roles of the individual WH2 motifs, we compared the activity of constructs with zero, one, two or three WH2 motifs (Figs. 1a, c; constructs VCD, W_1-C, W_2-C, W_3-C, respectively). In this series, activity decreased in the following order: W_3-C > W_2-C $\gg$ VCD > W_1-C. Thus, proteins containing three or two WH2 motifs had appreciably higher activity than those with fewer. A single WH2 motif appears to inhibit activity relative to the bare VCD (see below). Although these activities could in principle reflect differences in rates of actin filament elongation (e.g. by binding of the WH2 motifs to the filament barbed end[36]), Dominguez and colleagues observed that VopL did not change elongation rates in single filament assays[37]. Thus, the differences in activity likely reflect differences in nucleation potency. Together, these data demonstrate that actin binding by the WH2 motifs alone is insufficient to promote nucleation, and both the WH2 motifs and VCD play important roles in VopL function.

The VopL VCD is a U-shaped dimer stabilized by a coiled-coil

The W_3-C and VCD proteins form high affinity dimers in solution, based on multi-angle laser light scattering (MALLS) analyses (Fig 2a). We crystallized the VCD in space group $P2_12_12_1$ with two molecules in the asymmetric unit, and determined its structure to 2.36 Å resolution. Data collection and structure refinement statistics are listed in Table 1. Both molecules in the asymmetric unit are well-defined in the electron density map, except for residues 323-338. The VCD is mainly α-helical except for two anti-parallel β strands formed by residues 355-360 and 364-369 (Fig. 3a). Each subunit is composed of three structural regions, which we name the “arm”, “base” and “C-helix”, respectively, based on the shape of the structure shown in Figure 3a. The base consists of residues 244-278 and 395-456, and forms an elongated cluster of five α-helices. The arm is essentially an insert in the base that

consists of residues 283-384. These form a bundle of three helices capped distally to the base by the two-stranded β-sheet, and with an additional perpendicular helix proximal to the base. Finally, the C-helix (residues 462-484) emerges perpendicularly to the end of the arm opposite to the base.

There are two potential dimers in the asymmetric unit of the VCD crystals (Figs. 3a and S3). One is formed by coiled-coil interactions between the C-helices of the two subunits, and by contacts between the adjacent ends of the base (Fig. 3a). The second is formed by contacts between the arm from one monomer and the base from another monomer (Supplementary Fig. 3). The former dimer has an appreciably larger (1065 $Å^2$ versus 780 $Å^2$ buried) and more hydrophobic intermolecular interface, and is predicted by PDBePISA (Protein Interfaces, Surfaces and Assemblies)[38] to be the more probable of the two possibilities (complexation significance score of 0.2 versus 0.0). Moreover, a VopL protein lacking the C-helix (VCDΔh, residues 247-460) is monomeric in solution by MALLS analysis (Fig. 2b). Thus, both the structure and mutagenesis data support the functional relevance of the coiled-coil mediated dimer of Figure 3a, and we base our further analyses on it.

The VopL dimer forms a shallow U shape, with a wide platform formed by end to end association of the base, flanked by the perpendicular arm of each subunit (Fig. 3a). The C-terminal coiled coil extends perpendicularly from the center of the base. The N-terminus of the structure is at the base-arm elbow; the WH2 element would emerge from the VCD at this location. As discussed below, a 24 residue linker connects the first ordered residue in the structure with the C-terminus of WH2c. At the intermolecular interface a hydrophobic pocket formed by residues Thr422, Ala426, Leu465 of one molecule partially surrounds the sidechain of Tyr462 in the neighboring molecule (Fig. 3b). The sidechains of Lys421 and Gln418 hydrogen bond to those of Glu417 and Thr422 from the other chain. The C-terminal coiled coil is mediated by packing of the Leu465, Val469, Leu472, Leu476, Leu479 and Leu483 sidechains of the two monomers (Fig. 3c). The Arg468 sidechain also hydrogen bonds to the Glu473 sidechain across this interface.

The base is very similar in structure for each molecule in the asymmetric unit, with all-atom root mean square deviation (rmsd) of 0.36 Å. The same is true of the arm, with rmsd of 0.85 Å. However, the organization of the two domains differs between the two subunits due to rigid body movement about the interdomain hinge (residues 279-283 and 384-395, Supplementary Fig. 4). Thus, in solution VopL likely samples a range of conformations involving fluctuations in the relative orientation of the base and the arm. This notion is consistent with small angle x-ray scattering data by Dominguez and colleagues that suggest an average co-linear organization of the base and arm in solution [37].

Dimerization and actin contacts of the VCD are important for activity

Compared to the inactive W_3 protein, the highly active W_3-C protein is both dimeric (Fig. 2a) and contains additional potential contact sites to actin. To better dissect these two contributions to activity we performed three different experiments: artificial dimerization of WH2 proteins, mutagenic monomerization of W_3-C and increasing the number of WH2 motifs in a linear sequence. In the first experiments, we replaced the C terminal domain of WH2-containing constructs with glutathione S-transferase (GST), which forms high affinity

dimers[24]. At a concentration of 50 nM, the engineered W_3-GST protein exhibits substantial nucleation activity, which is comparable to that of W_2-C (Fig. 2c). Both W_2-GST and W_1-GST are inactive at this concentration. Similar behaviors are observed in N-terminal GST fusions (data not shown). Thus, dimerization alone can greatly increase the activity of W_3, which is completely inactive as a monomer even at high concentrations. Nevertheless, W_3-GST and W_2-GST remain appreciably less active than their native counterparts dimerized by the VCD. In the second experiments we found that while the activity of the monomeric W_3-CΔh is substantially below that of the dimeric W_3-C counterpart, the former protein is still more active than W_3 alone (Fig. 4a). This residual activity does not appear to result from residual dimerization, as a W_3-CΔh protein that also contains K421E and T422A mutations (W_3-CΔh_{KT}) designed to weaken dimerization contacts between the base is similarly active (Supplementary Fig. 5). Finally, we generated a W_4 construct by adding an additional WH2 motif to the N terminus of W_3. As shown in Figure 1b, W_4 proved to be completely inactive. Together, the data suggest that a specific spatial organization of the WH2 motifs, rather than merely their total number, is likely important for function. Moreover, while dimerization of the WH2 element is necessary for high activity, the VCD appears to contribute in ways beyond mere dimerization, perhaps through an ability to bind and orient actin molecules to favor nucleation (see below). Thus, the data imply a specific organization of actin in the nucleus, generated by the WH2 elements juxtaposed by the VCD.

To test the hypothesis that the VCD might contact actin, we mutated residues at the distal end of the arm and at the base of the VCD “U” structure. Residues Lys323, Arg347 and Arg354 form a conserved basic patch at the distal end of the arm (Fig. 3a). Mutations of these three residues to glutamic acid in W_3-C (construct W_3-C_{KRR}) or the VCD alone (construct VCD_{KRR}) substantially decreased activity (Figs. 4b, Supplementary Fig. 6, respectively). We also mutated to glycine the three residues Asp326, Val327 and Pro333 in the loop Tyr322-Gly338 near the end of the arm (constructs W_3-C_{DVP} and VCD_{DVP}, Fig. 3a), which is not observed in the electron density and is likely flexible in solution. These mutations also produced a small decrease in activity (Figs. 4b and S6). Thus, the distal end of the arm appears to contact actin during nucleation.

The surface of the base that faces into the VCD “U” consists of three distinct patches: a basic patch containing residues Lys421, Tyr425, and Arg428; an acidic patch containing Glu408, Asp413, and Glu417; and a mixed patch containing Leu249 and Glu251 (Supplementary Fig. 7). Mutation of the first patch (KYR to AAD (W_3-C_{KYR}) or to KAD (W_3-C_{YR})), or second patch (EDE to KKA (W_3-C_{EDE})) produced small but reproducible decreases in activity (Fig. 4c). Mutation of the third patch had no effect on activity (data not shown). Thus, the base may also contact actin during nucleation, although these interactions do not appear as important for activity as those to the arm.

Multi-angle laser light scattering analyses indicate that the wild type and mutant proteins are largely (and similarly) dimeric at concentrations as low as 500 nM (Supplementary Fig. 8a). In addition, the activities of several VopL proteins are proportional to concentration between 5 nM and 50 nM, suggesting the proteins are mostly dimeric even at low concentrations (Supplementary Fig. 8b). These data support the argument that the mutations perturb contacts to actin rather than causing loss of dimerization. Together, our biochemical

analyses suggest the VCD likely plays a direct role in organizing actin monomers in the VopL nucleus, in addition to dimerizing and orienting the WH2 elements.

VopL activity is sensitive to the length of linker between WH2c and C

It is somewhat paradoxical that W_1-C has lower activity than both W_2-C and VCD (Fig. 1c). That is, adding one WH2 motif to the VCD is inhibitory but adding two WH2 motifs is stimulatory. We hypothesized that this effect might arise because the natural 24-residue linker between the C-terminus of WH2c (Thr223, of the basic sequence LRKT) and the beginning of the VCD (Arg247) is too short, causing sub-optimal orientation of the initial bound actin monomer(s). To test this idea, we inserted 9- and 40-residue linkers into W_1-C, to give a total of 33 and 64 residues, respectively, between the WH2c motif and VCD (W_1-9-C and W_1-40-C, Fig. 1a). The linker in W_1-40-C is identical in length to that between WH2b and the C-terminus of W_2-C. As shown in Figure 5, increasing linker length in W_1-C progressively increases activity. In related experiments, when the WH2c motif in W_2-C or W_3-C is replaced by an equal length Gly-Gly-Ser linker (to give constructs W_1-L-C and W_2-L-C), activity decreases only modestly. Thus, a smaller number of WH2 motifs (e.g. W_3-C versus W_2-L-C) can be largely compensated for by increasing the spacing of those motifs from the VCD. These results are consistent with the idea that the natural linker between WH2c and C is too short (in one or both molecules in the dimer), likely preventing optimal organization of actin monomers for nucleation activity.

Discussion

Our data demonstrate that multiple WH2 motifs and the VCD of VopL are both required for high potency actin filament nucleation. Dimerization, either by the VCD or artificially by GST, is necessary for the WH2 motifs to nucleate. The VCD itself also appears to contact actin, since it alone can nucleate weakly, and mutagenesis of conserved residues in the base and arm decreases activity. These key data, along with the geometry of the VCD structure, suggest a preliminary model for the actin nucleus assembled by VopL. A central concept in this model is that the WH2 motifs recruit actin monomers, while the VCD provides organization that leads to a productive nucleus.

The requirement for dimerization of the WH2 element suggests that in the nucleus, at least one actin monomer is contributed or recruited by each subunit. An individual multi-WH2 protein should be able to assemble a single strand of the nascent paired actin filament (i.e. stabilize long-pitch contacts between actin monomers). But such activity is evidently insufficient for nucleation by VopL. This observation suggests that in VopL dimers, the paired WH2 elements act by stabilizing lateral (short-pitch) actin-actin contacts. Thus, the nucleus should minimally contain a short-pitch actin dimer.

How might such a structure interact with the VCD? One possibility is suggested by geometric considerations. In a short pitch actin dimer, the two subunits are axially displaced on average by 27.5 Å[39]. In the VCD, the distal end of the arm is ~30 Å from the platform created by the base. Thus, the axial displacement of an actin dimer could be accommodated by only small changes in the structural organization of the VCD. In this configuration the penultimate actin monomer would contact the distal end of the arm and the terminal

monomer would contact the base (Fig. 6). While our image in Figure 6 has the plane of the terminal monomer perpendicular to the plane of the VCD, other orientations with more acute angles are also possible. Such an arrangement would be consistent with several observations. First, the VCD alone has nucleation activity, suggesting that it may contact both actins in a short pitch dimer. Our mutagenesis data (Fig. 4b) suggest that residues at both the distal end of the arm and the VCD base formed by base contribute to nucleation activity, probably through contacts to actin. Second, in order for WH2c to bind this penultimate actin, the WH2c-VCD linker would need to extend from the N-terminus of the VCD, around the arm to its tip, a distance of ~50 Å, and then approximately half the length of an actin monomer to the N-terminus of the WH2 motif[35], ~28 Å. While these distances are obviously very approximate, they would be consistent with the idea that the natural 24 residue linker (~80 Å fully extended) may be poorly able to position a WH2c-bound actin on the VCD, explaining the low activity of W_1-C, and the progressive increase in activity as the linker is lengthened (Fig. 5). In native VopL, the penultimate monomer may be recruited by WH2b. Third, SAXS analyses from Dominguez and colleagues on the W_1-C:actin complex suggest that an ordered actin contacts the base [37]. This terminal monomer could be recruited by the WH2c of the opposing VCD. Finally, the short-pitch dimer bound to the VCD would be further stabilized by additional actin monomers recruited by additional WH2 motifs, consistent with the activity series W_3-C > W_2-C > W_1-L-C (Fig. 5). While this model remains speculative, it makes testable predictions that will be explored in future work.

The stabilization of short-pitch contacts in the nascent actin filament appears to be a common feature of WH2-based nucleation factors, both prokaryotic and eukaryotic. In Cobl and Lmod, the stoichiometry of actin binding and linker length dependencies of activity have led to models in which WH2 and other motifs stabilize a short-pitch actin trimer[8,9]. In Spire, a tandem array of WH2 motifs was shown by electron microscopy to organize a linear actin structure, which was proposed to nucleate through serving as a single, long-pitch strand of an actin filament[7]. However, Spire alone is a relatively weak nucleation factor, whose activity is appreciably enhanced through dimerization mediated by the formin protein, Cappuccino[40]. Similarly, the actin nucleation factor TARP from the pathogen *Chlamydia trachomatis* requires oligomerization of its WH2 motif by an adjacent poly-proline region for activity[33]. In both Spire and TARP, higher potency likely arises, as in VopL, from the ability of dimers to organize lateral contacts between actin monomers in the nascent filament. These experimental findings are all consistent with computational analyses of actin nucleation, which suggest that a stabilized short-pitch dimer will recruit a third monomer with much greater affinity than will a long-pitch dimer[4]. Thus, short-pitch dimers should act as more effective nuclei.

Together, our findings provide an initial mechanistic model for the potent actin nucleation activity of VopL. Yet many questions remain to be answered. What is the conformation of the VopL-bound actin nucleus, and what contacts to both WH2 motifs and the VCD stabilize it? Does VopL remain bound to filaments after nucleation? If so, does it bind filament ends or sides; does it remain static like the Arp2/3 complex or process like formins? If not, what triggers its release from the nascent filament? Why do VopL and VopF, which presumably

nucleate through very similar mechanisms, produce different actin structures in cells? Our work here provides an initial framework to address these questions and others in the future.

Methods

Molecular Biology and Protein Purification

We cloned VopL fragments (W_3-C: 115–484, W_2-C: 155–484, W_1-C: 194–484, VCD: 247–484 and WH2 peptides: WH2a: 129–157, WH2b: 158–187, WH2c: 199–226, W_3: 115–246) into pGEX vector by PCR and verified them by DNA sequencing. Proteins were expressed in *Escherichia coli* BL21(DE3) $T1^R$ cells grown in LB media and induced with 1mM IPTG at optical density (OD_{600}) of 0.8. Proteins were purified with successive glutathione-sepharose affinity chromatography, tobacco etch virus (TEV) protease cleavage, followed by strong anion exchange and gel filtration chromatographies. GST fusions of VopL WH2 fragments (W_3-GST, W_2-GST and W_1-GST respectively) were expressed from pET11a and purified using glutathione-sepharose affinity, strong anion exchange and gel filtration chromatographies.

Actin Polymerization Assay

Actin was prepared from rabbit muscle. All actin polymerization assays contained 4μM actin (5% pyrene labeled) and 5 nM–500 nM VopL proteins in KMEI-G Buffer (10 mM Imidazole (pH 7.0), 50 mM KCl, 1 mM $MgCl_2$, and 1 mM EGTA), and were performed at 20 ° C as decribed[41]. Assays were performed using a Jobin Yvon Horiba Fluorimeter (www.jyhoriba.com). The half-time ($t_{1/2}$) of actin assembly was measured as the time for 50% polymerization.

Protein Crystallization and X-ray Diffraction Data Collection

VCD crystals (50 × 150 × 200 μm) were grown at 20°C using the hanging-drop vapor-diffusion method. Drops contained 1 μl of 10–15 mg ml^{-1} protein solution (20 mM Tris, pH 7.5, 100 mM NaCl, 1 mM DTT) plus 1 μl of reservoir solution (100 mM Tris pH 7.5, 20% PEG 1500 (w/v)) and were equilibrated against 200μl of reservoir solution. Crystals of selenomethionine-labeled protein were obtained under similar conditions. Crystals were cryoprotected by addition of 30% (v/v) ethylene glycol to reservoir solution. Native crystals were soaked in a cryosolution that also contained 5% PEG20,000 (w/v) for 30 minutes prior to flash cooling. Native and anomalous dispersion data were collected at the Advanced Photon Source 19ID beamline at 100 K. Native VCD crystallized in space group $P2_12_12_1$ with unit cell parameters of a = 56 Å, b =88 Å, c = 101 Å, containing two molecules in each asymmetric unit with ~50% solvent. Crystals diffracted X-rays to a minimum Bragg spacing of 2.30 Å. Data indexing and scaling were carried out using the HKL3000 suite of programs[42]. Data collection statistics are in Table 1.

Phase Determination and Structure Refinement

We used multi-wavelength anomalous diffraction data to a resolution of 3.1–3.21 Å from a selenomethionine VopL crystal to obtain experimental phases. The peak, reflection and remote wavelengths were 0.9794 Å, 0.9795 Å and 0.9717 Å, respectively. Ten of ten expected selenium sites were located using the program SHELXD[43]. Phases were refined

with the program MLPHARE[44] and further improved to a figure-of-merit of 0.90 by density modification using the program DM[45]. An initial structure model was built using the program Buccaneer[46] and further improved by manual model building using the program Coot[47]. We collected a native data set at the same temperature and beamline, at a wavelength of 0.9792 Å. An electron density map of native VopL was obtained through molecular replacement using the selenomethionine VopL as a search model using the program Phaser[48]. The native structure model was again initially built using Buccaneer and improved with manual model building. Structure refinement with native data was carried out using the program PHENIX[49], consisting of refinements of individual sites, individual B-factors and TLS parameters. The current model contains two VopL chains in one asymmetric unit. Statistics of refinement and structural quality are listed in Table 1. In the refined structure, 97.5%, 2.5% and 0.0% of residues are in the favored, allowed and disallowed regions of the Ramachandran plot, respectively, according to the Molprobity structural validation tools[50].

Multi-Angle Laser Light Scattering (MALLS)

We applied 500 μl of 40 μM VopL proteins at a flow rate of 0.5 ml min^{-1} to either a Superdex 200 10/300 or a Superdex 75 10/300 column (Amersham Biosciences) equilibrated in buffer containing 20 mM Tris pH 8.0, 100 mM NaCl and 2 mM DTT. The chromatography column was combined in line with a three angle light scattering detector (miniDAWN TREOS) coupled to a refractive index detector (Optilab rEX, Wyatt Technology). Data analysis and molecular weight calculations were carried out using the program ASTRA V (Wyatt technology).

Isothermal Titration Calorimetry (ITC)

All ITC experiments were performed using a VP-ITC MicroCalorimeter at 20°C. Prior to each experiment, WH2 peptides and actin were dialyzed extensively in the same beaker against 2 liters of G-Buffer for at least 24 hours. G-Buffer contains 2 mM Tris, pH 8.0, 0.1 mM $CaCl_2$, 0.5 mM DTT, 1 mM NaN_3 and 0.2 mM ATP. In each experiment, 100 μM of WH2 peptide was titrated into 10 μM actin in G-Buffer. Data were analyzed and fit to a single site model using the program Origins7, Microcal for ITC.

Supplementary Material

Refer to Web version on PubMed Central for supplementary material.

Acknowledgments

We thank Jacob Zahm[1,2] for acquiring the data in Figure S7b and for discussion, Zbyszek Otwinowski, Dominika Borek and participants in the 2010 CCP4 workshop, especially P. Afonine, G. Murshudov and B. Lohkamp, for technical assistance with protein structure determination, F. Correa[1] for assistance with MALLS experiments and data analysis, Z. Chen and S. Padrick for discussion. Results shown in this report are derived from work performed at Argonne National Laboratory, Structural Biology Center at the Advanced Photon Source. Argonne is operated by UChicago Argonne, LLC, for the U.S. Department of Energy, Office of Biological and Environmental Research under contract DE-AC02-06CH11357. Work was supported by funds from the Howard Hughes Medical Institute and a Welch Foundation grant to M.K.R. (I-1544).

References

1. Le Clainche C, Carlier MF. Regulation of actin assembly associated with protrusion and adhesion in cell migration. Physiol Rev. 2008; 88:489–513. [PubMed: 18391171]
2. Pollard TD, Borisy GG. Cellular motility driven by assembly and disassembly of actin filaments. Cell. 2003; 112:453–65. [PubMed: 12600310]
3. Chhabra ES, Higgs HN. The many faces of actin: matching assembly factors with cellular structures. Nat Cell Biol. 2007; 9:1110–21. [PubMed: 17909522]
4. Sept D, McCammon JA. Thermodynamics and kinetics of actin filament nucleation. Biophys J. 2001; 81:667–74. [PubMed: 11463615]
5. Pruyne D, et al. Role of formins in actin assembly: nucleation and barbed-end association. Science. 2002; 297:612–5. [PubMed: 12052901]
6. Machesky LM, Atkinson SJ, Ampe C, Vandekerckhove J, Pollard TD. Purification of a cortical complex containing two unconventional actins from Acanthamoeba by affinity chromatography on profilin-agarose. J Cell Biol. 1994; 127:107–15. [PubMed: 7929556]
7. Quinlan ME, Heuser JE, Kerkhoff E, Mullins RD. Drosophila Spire is an actin nucleation factor. Nature. 2005; 433:382–8. [PubMed: 15674283]
8. Ahuja R, et al. Cordon-bleu is an actin nucleation factor and controls neuronal morphology. Cell. 2007; 131:337–50. [PubMed: 17956734]
9. Chereau D, et al. Leiomodin is an actin filament nucleator in muscle cells. Science. 2008; 320:239–43. [PubMed: 18403713]
10. Chesarone MA, Goode BL. Actin nucleation and elongation factors: mechanisms and interplay. Curr Opin Cell Biol. 2009; 21:28–37. [PubMed: 19168341]
11. Renault L, Bugyi B, Carlier MF. Spire and Cordon-bleu: multifunctional regulators of actin dynamics. Trends Cell Biol. 2008; 18:494–504. [PubMed: 18774717]
12. Goley ED, Welch MD. The ARP2/3 complex: an actin nucleator comes of age. Nat Rev Mol Cell Biol. 2006; 7:713–26. [PubMed: 16990851]
13. Pollard TD. Regulation of actin filament assembly by Arp2/3 complex and formins. Annu Rev Biophys Biomol Struct. 2007; 36:451–77. [PubMed: 17477841]
14. Robinson RC, et al. Crystal structure of Arp2/3 complex. Science. 2001; 294:1679–84. [PubMed: 11721045]
15. Otomo T, et al. Structural basis of actin filament nucleation and processive capping by a formin homology 2 domain. Nature. 2005; 433:488–94. [PubMed: 15635372]
16. Xu Y, et al. Crystal structures of a Formin Homology-2 domain reveal a tethered dimer architecture. Cell. 2004; 116:711–23. [PubMed: 15006353]
17. Shemesh T, Otomo T, Rosen MK, Bershadsky AD, Kozlov MM. A novel mechanism of actin filament processive capping by formin: solution of the rotation paradox. J Cell Biol. 2005; 170:889–93. [PubMed: 16157699]
18. Vavylonis D, Kovar DR, O'Shaughnessy B, Pollard TD. Model of formin-associated actin filament elongation. Mol Cell. 2006; 21:455–66. [PubMed: 16483928]
19. Dominguez R. Structural insights into de novo actin polymerization. Curr Opin Struct Biol. 20:217–25. [PubMed: 20096561]
20. Ghosh P. Process of protein transport by the type III secretion system. Microbiol Mol Biol Rev. 2004; 68:771–95. [PubMed: 15590783]
21. Orth K. Function of the Yersinia effector YopJ. Curr Opin Microbiol. 2002; 5:38–43. [PubMed: 11834367]
22. Aktories K, Barbieri JT. Bacterial cytotoxins: targeting eukaryotic switches. Nat Rev Microbiol. 2005; 3:397–410. [PubMed: 15821726]
23. Cheng HC, Skehan BM, Campellone KG, Leong JM, Rosen MK. Structural mechanism of WASP activation by the enterohaemorrhagic E. coli effector EspF(U). Nature. 2008; 454:1009–13. [PubMed: 18650809]
24. Padrick SB, et al. Hierarchical regulation of WASP/WAVE proteins. Mol Cell. 2008; 32:426–38. [PubMed: 18995840]

25. Campellone KG, Robbins D, Leong JM. EspFU is a translocated EHEC effector that interacts with Tir and N-WASP and promotes Nck-independent actin assembly. Dev Cell. 2004; 7:217–28. [PubMed: 15296718]
26. Sallee NA, et al. The pathogen protein EspF(U) hijacks actin polymerization using mimicry and multivalency. Nature. 2008; 454:1005–8. [PubMed: 18650806]
27. Suzuki T, et al. Neural Wiskott-Aldrich syndrome protein (N-WASP) is the specific ligand for Shigella VirG among the WASP family and determines the host cell type allowing actin-based spreading. Cell Microbiol. 2002; 4:223–33. [PubMed: 11952639]
28. Fradelizi J, et al. ActA and human zyxin harbour Arp2/3-independent actin-polymerization activity. Nat Cell Biol. 2001; 3:699–707. [PubMed: 11483954]
29. Tripathi R, et al. VopF, a type III effector protein from a non-O1, non-O139 Vibrio cholerae strain, demonstrates toxicity in a Saccharomyces cerevisiae model. J Med Microbiol. 59:17–24. [PubMed: 19779031]
30. Liverman AD, et al. Arp2/3-independent assembly of actin by Vibrio type III effector VopL. Proc Natl Acad Sci U S A. 2007; 104:17117–22. [PubMed: 17942696]
31. Haglund CM, Choe JE, Skau CT, Kovar DR, Welch MD. Rickettsia Sca2 is a bacterial formin-like mediator of actin-based motility. Nat Cell Biol. 12:1057–63. [PubMed: 20972427]
32. Tam VC, Serruto D, Dziejman M, Brieher W, Mekalanos JJ. A type III secretion system in Vibrio cholerae translocates a formin/spire hybrid-like actin nucleator to promote intestinal colonization. Cell Host Microbe. 2007; 1:95–107. [PubMed: 18005688]
33. Jewett TJ, Fischer ER, Mead DJ, Hackstadt T. Chlamydial TARP is a bacterial nucleator of actin. Proc Natl Acad Sci U S A. 2006; 103:15599–604. [PubMed: 17028176]
34. Tam VC, et al. Functional Analysis of VopF Activity Required for Colonization in Vibrio cholerae. MBio. :1.
35. Chereau D, et al. Actin-bound structures of Wiskott-Aldrich syndrome protein (WASP)-homology domain 2 and the implications for filament assembly. Proc Natl Acad Sci U S A. 2005; 102:16644–9. [PubMed: 16275905]
36. Co C, Wong DT, Gierke S, Chang V, Taunton J. Mechanism of actin network attachment to moving membranes: barbed end capture by N-WASP WH2 domains. Cell. 2007; 128:901–13. [PubMed: 17350575]
37. Namgoong SBM, Glista MJ, Winkelman JD, Rebowski G, Kovar DR, Dominguez R. Mechanism of Actin Filament Nucleation by Vibrio VopL – Implications for Tandem W Domain-Based Nucleation. Nat Struct Mol Biol. 2011 in press.
38. Krissinel E, Henrick K. Inference of macromolecular assemblies from crystalline state. J Mol Biol. 2007; 372:774–97. [PubMed: 17681537]
39. Holmes KC, Popp D, Gebhard W, Kabsch W. Atomic model of the actin filament. Nature. 1990; 347:44–9. [PubMed: 2395461]
40. Quinlan ME, Hilgert S, Bedrossian A, Mullins RD, Kerkhoff E. Regulatory interactions between two actin nucleators, Spire and Cappuccino. J Cell Biol. 2007; 179:117–28. [PubMed: 17923532]
41. Leung DW, Morgan DM, Rosen MK. Biochemical properties and inhibitors of (N-)WASP. Methods Enzymol. 2006; 406:281–96. [PubMed: 16472665]
42. Minor W, Cymborowski M, Otwinowski Z, Chruszcz M. HKL-3000: the integration of data reduction and structure solution--from diffraction images to an initial model in minutes. Acta Crystallogr D Biol Crystallogr. 2006; 62:859–66. [PubMed: 16855301]
43. Schneider TR, Sheldrick GM. Substructure solution with SHELXD. Acta Crystallogr D Biol Crystallogr. 2002; 58:1772–9. [PubMed: 12351820]
44. Otwinowski, Z. Isomorphous Replacement and Anomalous Scattering Proceedings of CCP4 Study Weekend; 1991. p. 80-86.
45. Wilson R, et al. 2.2 Mb of contiguous nucleotide sequence from chromosome III of C. elegans. Nature. 1994; 368:32–8. [PubMed: 7906398]
46. Cowtan K. The Buccaneer software for automated model building. 1. Tracing protein chains. Acta Crystallogr D Biol Crystallogr. 2006; 62:1002–11. [PubMed: 16929101]

47. Emsley P, Cowtan K. Coot: model-building tools for molecular graphics. Acta Crystallogr D Biol Crystallogr. 2004; 60:2126–32. [PubMed: 15572765]

48. McCoy AJ, et al. Phaser crystallographic software. J Appl Crystallogr. 2007; 40:658–674. [PubMed: 19461840]

49. Adams PD, et al. PHENIX: building new software for automated crystallographic structure determination. Acta Crystallogr D Biol Crystallogr. 2002; 58:1948–54. [PubMed: 12393927]

50. Davis IW, Murray LW, Richardson JS, Richardson DC. MOLPROBITY: structure validation and all-atom contact analysis for nucleic acids and their complexes. Nucleic Acids Res. 2004; 32:W615–9. [PubMed: 15215462]

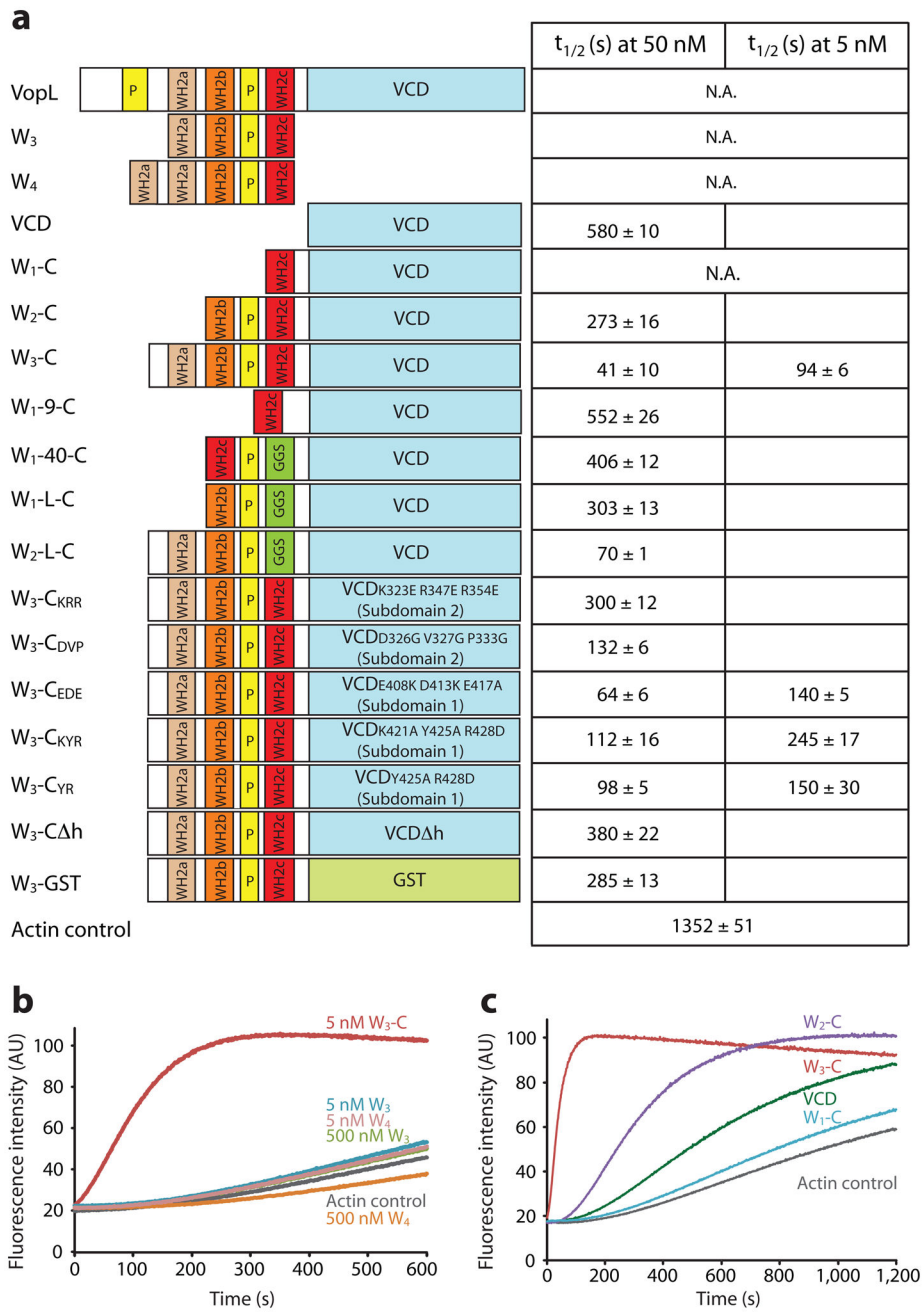

Figure 1.

Both the WH2 motifs and VCD contribute to actin nucleation by VopL. (**a**) Domain structures of VopL constructs used in this work. All constructs lack the N-terminal secretion sequence needed for VopL translocation into host cells, whose deletion does not affect activity (not shown). P: Proline-rich motif. WH2: WASP Homology 2 domain. VCD: VopL C-terminal domain. GGS: (Gly-Gly-Ser) linker. The half-time ($t_{1/2}$) of actin assembly for each VopL protein is given by the average and standard deviation measured in three experiments. Assays contained 50 nM or 5 nM VopL proteins, as indicated. (**b**) Actin assembly assays contained the indicated concentrations of VopL constructs W_3-C, W_3 or

W_4. (**c**) Actin assembly assays contained 50 nM W_3-C, W_2-C, W_1-C or VCD. Figures in this manuscript were all generated using Adobe Illustrator CS2.

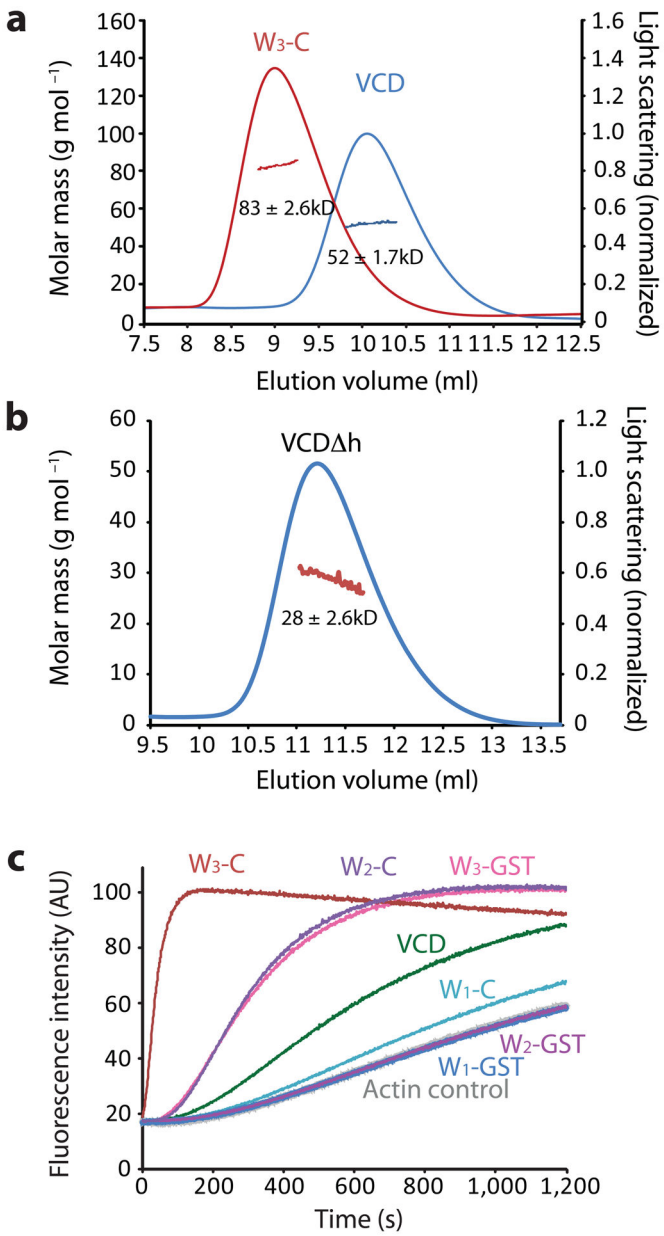

Figure 2.

Dimerization is necessary for actin nucleation by the VopL WH2 motifs. (**a**) Size exclusion chromatography—multi-angle laser light scattering (MALLS) analysis of VopL constructs W_3-C (red) and VCD (blue). Normalized scattered light in the chromatographic elution (right y-axis) is superimposed on the molecular weight distribution (left y-axis). (**b**) MALLS analysis of VCDΔh. Data plotted as in (**a**). (**c**) Actin polymerization assays performed with 4 μM actin and 50 nM W_3-C, W_2-C, W_1-C, VCD, W_3-GST, W_2-GST or W_1-GST.

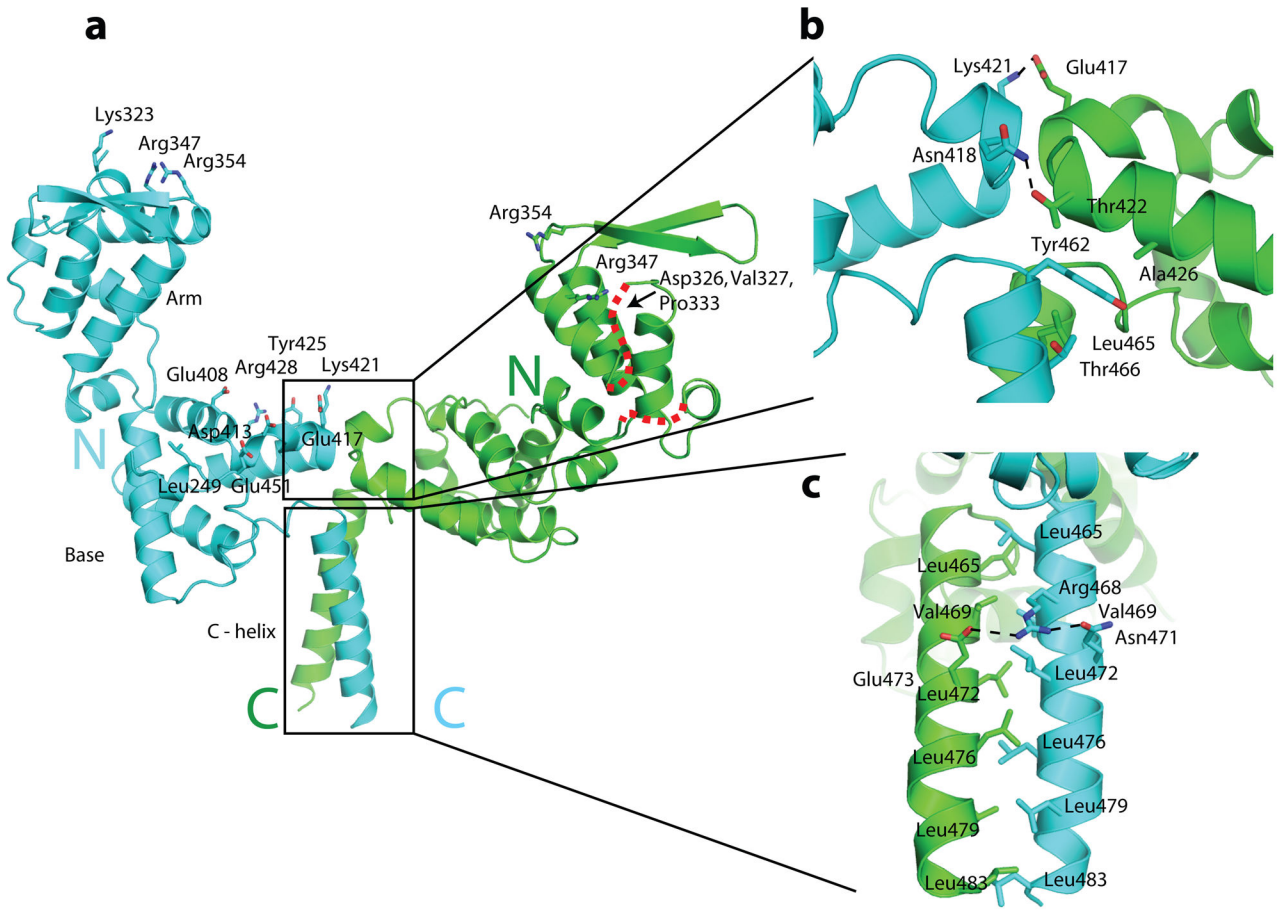

Figure 3.

Structure of the VCD dimer. (**a**) Ribbon diagram of the structure; monomers are colored blue and green. The N- and C-termini of each monomer are indicated. Red dashed lines indicate regions not observed in the electron density map for the green monomer (analogous regions not shown in the blue monomer). Boxed regions are enlarged in (**b**) and (**c**), which show detailed views of dimer interface. Black dashed lines indicate hydrogen bonds. In all panels sidechains of residues discussed in the text are shown as sticks.

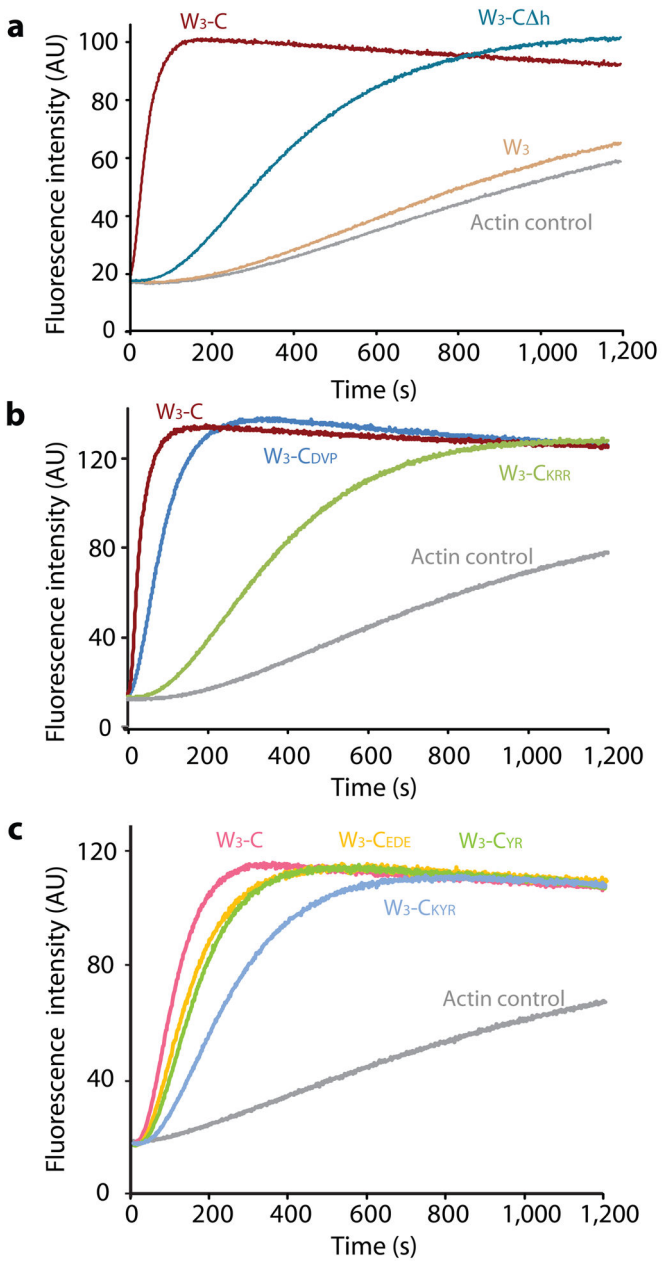

Figure 4.

The VCD contributes to actin assembly activity by dimerization and contacts to actin. Assays were performed with 4 μM actin and 50 nM (**a**, **b**) or 5 nM (**c**) of the indicated VopL proteins. (**a**) Comparison of W_3-C, W_3-CΔh and W_3. (**b**) Comparison of W_3-C with the VCD arm mutants, W_3-C_{KRR} and W_3-C_{DVP}. (**c**) Comparison of W_3-C with the VCD base mutants, W_3-C_{KYR}, W_3-C_{YR} and W_3-C_{EDE}.

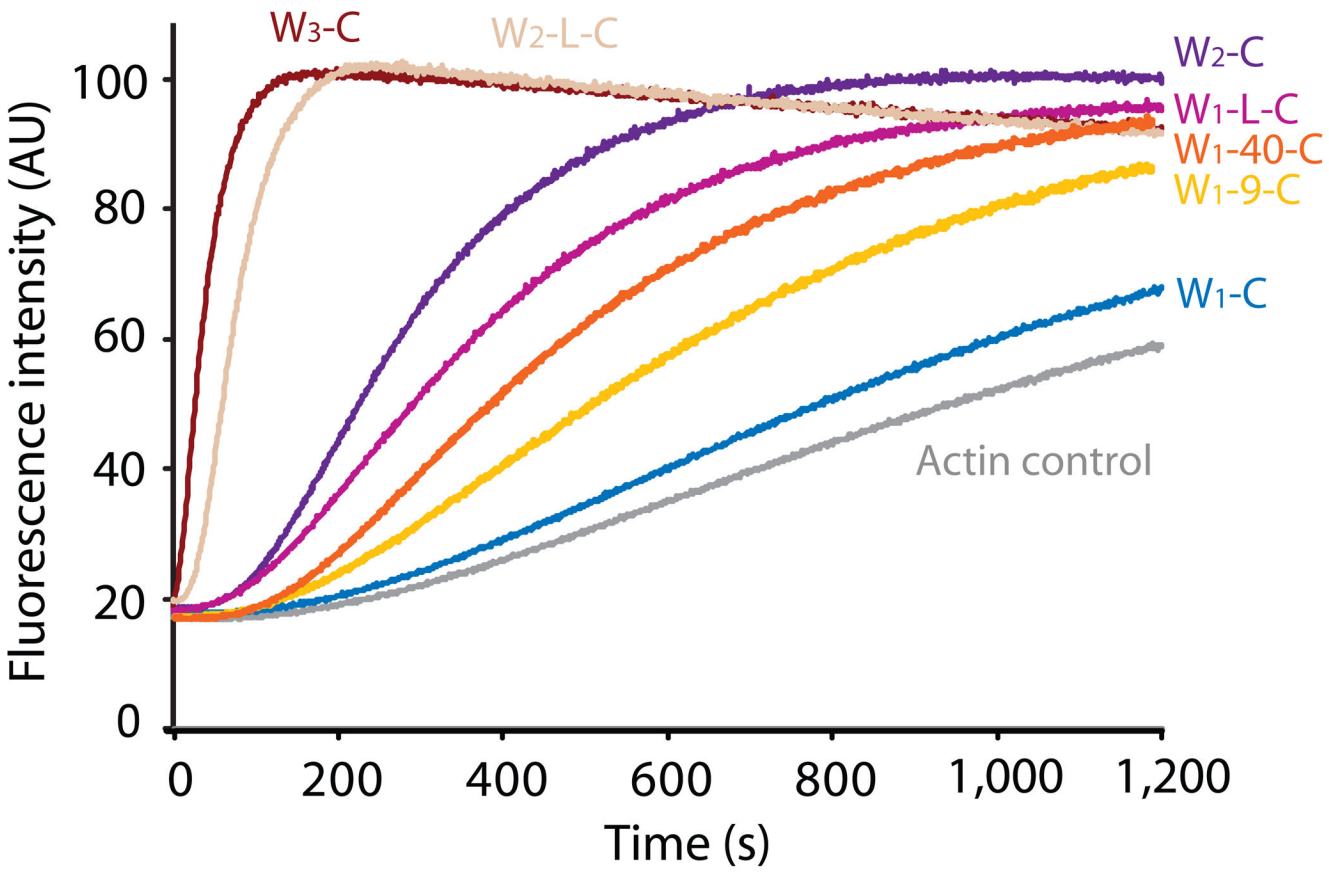

Figure 5.

Increasing the linker between WH2c and the VCD increases actin assembly activity. Assays contained of each 50 nM VopL protein, W_3-C, W_2-C, W_1-C, W_2-L-C or W_1-L-C.

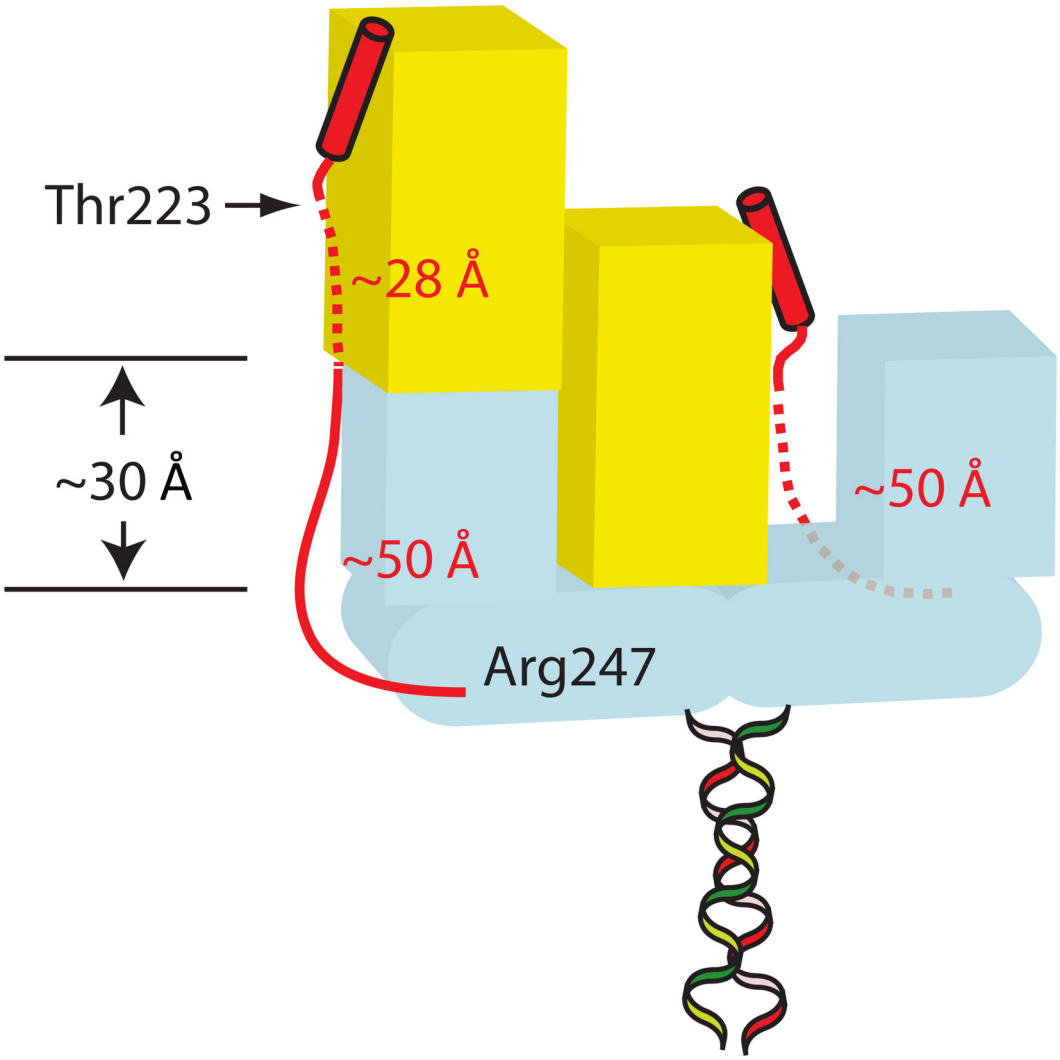

Figure 6.

Model for a minimal actin nucleus assembled by VopL. VCD is indicated by blue blocks with ribbons representing the coiled coil. Initial actin monomers are indicated by yellow boxes. Actin-bound WH2c motifs are shown as red cylinders. Red lines indicate linkers between WH2c and VCD. Additional actin monomers assembled by WH2a and WH2b would bind to the upper surfaces of the WH2c-bound actins, making additional short- and long-pitch contacts, further stabilizing the assembly. Actins are implicitly shown with barbed ends directed away from the VCD, but our current data do not speak to the orientation of actin monomers in the VopL nucleus.

Table 1

Data collection, phasing and refinement statistics

	Native VopL			Selenomethione-VopL			
Data collection							
Space group	$P2_12_12_1$			$P2_12_12_1$			
Cell dimensions							
a, b, c (Å)	55.15	89.81	102.98	56.19	88.64	101.36	
a, b, c (°)	90	90	90	90	90	90	
			Peak		*Inflection*		*Remote*
Wavelength	0.9792		0.9794	0.9795			0.9717
Resolution (Å)	50.0-2.30		50.0-3.10	50.0-3.17			50.0-3.21
Rmerge	0.034(0.618)		0.074(0.713)	0.075(0.788)			0.068(0.665)
I/σ(I)	26.4(1.4)		64.2(5.1)	40.5(3.8)			43.7(4.5)
Completeness (%)	99.1(99.0)		99.8(100)	99.9(100)			99.9(100)
Redundancy	2.8(2.5)		23.5(24.2)	11.8(11.9)			11.7(12.1)
Refinement							
Resolution (Å)	29-2.30						
No. reflections	23040						
Rwork/Rfree	0.221(0.276)/0.275(0.334)						
No. atoms							
Protein	3510						
Ligand/ion	9						
Water	36						
B-factors							
Protein	88.92						
Ligand/ion	115.4						
Water	64.9						
R.m.s deviations							
Bond lengths (Å)	0.003						
Bond angles (°)	0.564						

*One seleno-methionine and one native crystal were used for data collection.

* Values in parentheses are for highest-resolution shell.